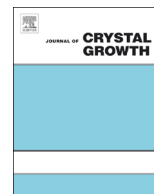




ELSEVIER

Contents lists available at ScienceDirect

Journal of Crystal Growth

journal homepage: www.elsevier.com/locate/jcrysgr

Temperature-dependent growth mechanism and microstructure of ZnO nanostructures grown from the thermal oxidation of zinc



Lu Yuan^a, Chao Wang^b, Rongsheng Cai^b, Yiqian Wang^b, Guangwen Zhou^{a,*}

^a Department of Mechanical Engineering & Multidisciplinary Program in Materials Science and Engineering, State University of New York, Binghamton, NY 13902, USA

^b The Cultivation Base for State Key Laboratory and College of Physical Science, Qingdao University, Qingdao 266071, China

ARTICLE INFO

Article history:

Received 26 September 2013

Received in revised form

12 December 2013

Accepted 19 December 2013

Communicated by A. Ohtomo

Available online 28 December 2013

Keywords:

A1. Crystal morphology

A1: Characterization

B1. Nanomaterials

B1. Zinc compounds

B1. oxides

ABSTRACT

We report a detailed study on the growth morphologies and microstructure of ZnO nanostructures formed from the oxidation of Zn at different temperatures. ZnO shows bicrystalline nanowire morphology for oxidation below the melting point of Zn, and single-crystalline morphology between the melting and boiling points of Zn, and tetrapod morphology above the boiling point of Zn. The morphological and microstructural variations are attributed to the temperature-dependent oxide growth mechanisms, i.e., the oxidation below the melting point of Zn is dominated by a solid–solid transformation process, a liquid–solid process between the melting and boiling points of Zn, and a vapor–solid process above the boiling point of Zn. The understanding of the oxide growth mechanisms from these results may have practical implications for rational control of the morphology, crystallinity, preferential growth directions, shape and aspect ratio of ZnO nanostructures

© 2013 Elsevier B.V. All rights reserved.

1. Introduction

Zinc oxide (ZnO) is a direct wide-bandgap semiconductor (3.37 eV) with large exciton binding energy (60 meV). ZnO has received intensive interest for its unique properties and wide applications in optics, optoelectronics, sensors, biomedical sciences actuators, energy, and spintronics [1–3]. Shrinking its size to the nanoscale is expected to open an even wider range of technical possibilities such as nanophotonics, nanoelectronics, and nanobiotechnology [4,5]. ZnO nanostructures with diverse morphologies have been produced, including wires [6,7], belts [8], tubes [9], rods [10], springs [11], rings [12], sheets [13], and tetrapods [14–16]. The approaches used for growing ZnO nanostructures mainly include vapor–solid [17–19], vapor–liquid–solid [20], epitaxial growth [21,22], hydrothermal [23], and solution processes [24]. More recently, thermal oxidation of Zn has been used to grow ZnO nanostructures [25–31]. Compared to the catalyst-assisted growth, direct oxidation of metallic zinc is a simple, cost effective and non-catalytic approach for producing ZnO nanostructures with large-scale growth capabilities and high purity owing to the elimination of intermediaries involved in catalytic chemical synthesis of oxide nanostructures.

Directly heating Zn foils or powders under oxygen gas flow results in the formation of various ZnO nanostructures with a large variety of morphologies [26,32,33]. Due to its capabilities of producing a rich variety of morphologies of nanostructures, the vapor–solid mechanism is usually invoked to understand the oxidation-induced ZnO nanostructure growth, in which Zn evaporates from the raw material and reacts with gaseous oxygen to form nanostructured ZnO [26,32,33]. The temperatures reported for ZnO nanostructure formation during oxidation vary typically from 400 to 1000 °C, which cover the melting temperature (420 °C) and boiling temperature (907 °C) of Zn. While Zn has a relatively high vapor pressure at these oxidation temperatures, particularly above the boiling temperature, the rapid oxidation of Zn to form a solid ZnO coating layer on the Zn substrate surface can effectively prevent further Zn evaporation from the Zn substrate. Meanwhile, decomposition of ZnO requires a temperature up to ~1400 °C [34], which is much higher than the oxidation temperatures (i.e., 400–1000 °C) typically employed for ZnO nanostructure growth. This implies that the growth of ZnO nanostructures should stop quickly soon after the formation of a solid ZnO coating layer on the Zn substrate, but this is actually not the case since many experimental results have demonstrated that a longer oxidation time results in the formation of more ZnO nanostructures on the Zn surface [35]. Such controversies suggest that the vapor–solid process may not be the only mechanism responsible for ZnO nanostructure formation during the oxidation of Zn. A detailed and clear understanding of the growth

* Corresponding author. Tel.: +1 6077775084; fax: +1 6077774620.

E-mail addresses: gzhou@binghamton.edu, zhougw@yahoo.com (G. Zhou).

mechanisms is essential for rational control of the morphology, crystallinity, preferential growth directions, shape and aspect ratio in an efficient way.

Motivated by the aforementioned questions and speculations, we perform a systematic study to ascertain the morphological and microstructure evolution of ZnO nanostructures during the oxidation of Zn substrates. Particularly, we examine the effect of oxidation temperature on ZnO nanostructure formation. Indeed, we find that the mechanism governing the formation of ZnO nanostructures actually depends on the oxidation temperature. At the oxidation temperature below the melting of Zn, the formation of ZnO nanostructures occurs via a solid–solid transformation mechanism, in which the relaxation of the compressive stresses generated by the volume mismatch accompanying the ZnO/Zn interfacial reaction stimulates the formation of bicrystalline ZnO nanowires. For oxidation at the temperature above the boiling point of Zn, ZnO nanostructures occur via the vapor–solid mechanism, in which Zn evaporates from the Zn substrate and reacts with gaseous oxygen to form solid ZnO that precipitates onto the surrounding areas. For oxidation at temperatures between the melting and boiling points of Zn, the liquid–solid mechanism is the dominating process that results in the formation of single crystalline ZnO nanowires on the Zn substrate.

2. Experimental details

High-purity Zn foils (99.99%) with a thickness of 0.25 mm obtained from Sigma-Aldrich are used in the oxidation experiments. Gold (~10 nm) coated Si(111) wafers serve as the deposition substrates that are placed next to the Zn foils. A chromium primer layer (~2 nm) is coated before Au coating to improve adhesion between the gold layer and the silicon substrate. The oxidation experiments are carried out in a horizontal tube furnace with pure oxygen (99.999%) as the reaction gas. Zn samples are first thoroughly rinsed with deionized water followed by ultrasonication in acetone for 5 min. The cleaned Zn substrate is dried in N₂ and then placed in a ceramic boat. The silicon substrate is placed in another ceramic boat. Those two ceramic boats are then put into the horizontal tube furnace with the silicon substrate upstream along the gas flow direction. Fig. 1 is a schematic diagram of the experimental setup. The purpose of placing a Si substrate next to the Zn foil is to examine if there is any ZnO nanostructure deposition onto the surrounding area, particularly upstream along the oxygen gas flow direction, which would provide significant insight regarding the vapor–solid mechanism for ZnO nanostructure formation during the oxidation of Zn. Before the oxidation experiment, the furnace is flowed with 100 sccm (standard cubic centimeter per minute) argon (Ar) gas for 5 min and then rapidly heated from room temperature to the desired temperature ranging from 200 °C to 1000 °C in 10 min with Ar gas flow. The oxidation of Zn is performed by switching quickly from the Ar gas flow to pure oxygen gas flow with a 100 sccm flow rate and the oxidation duration is 30 min. After oxidation, the furnace is then naturally cooled down to room temperature in the oxygen atmosphere. The as-synthesized products are characterized by field emission scanning electron

microscopy (FEG-SEM, FEI Supra 55VP) and transmission electron microscopy (JEOL JEM 2100 F) operated at 200 kV.

3. Results

Fig. 2 shows representative SEM images of the surfaces of the Zn foils oxidized at the different temperatures. The SEM observations show that no ZnO nanostructures are formed on the Zn substrate at relatively low oxidation temperatures (200 °C and 300 °C) (see Fig. 2(a) and (b)). The oxidation at 400 °C results in the formation of ZnO nanowires on the Zn surface, where the diameter of the nanowires is ~20 nm and the length is up to 500 nm (see Fig. 2(c)). As seen in Fig. 2(d), the oxidation at 500 °C results in the formation of ZnO nanowires with a much higher surface density, larger diameter (~50 nm) and longer length (~1.5 μm) compared to the lower oxidation temperature. Fig. 2(d) also shows that the oxidized Zn substrate becomes slightly roughened compared to the oxidation at the lower temperatures, which may be caused by surface melting of the Zn substrate at the oxidation temperature (the melting temperature of Zn is ~420 °C). For oxidation at 600 °C, the Zn surface becomes highly roughened with formation of taper-shaped ZnO nanowires having a diameter of 500 nm at the root and a length up to 2 μm (Fig. 2(e)). For oxidation at 800 °C, micro-sized ZnO rods are formed on the significantly roughened Zn surface. Those rods are tapered with a diameter up to 1.8 μm at the root region and a length up to several μm, indicating the significant radial growth in addition to the axial growth. For oxidation at 1000 °C, the Zn foil has totally disappeared from the ceramic boat where the Zn foil was originally placed, this is due to the fast evaporation of Zn at the high temperature above its boiling point (907 °C).

As described in the experimental section, another ceramic boat with a Si wafer inside was also placed next to the ceramic boat with the Zn foil inside. Examining the reaction product on the Si wafer would allow for elucidating if the vapor–solid process is involved in ZnO nanostructure formation, for which Zn is expected to evaporate from the Zn foil and reacts with oxygen gas to form ZnO nanostructures which are then deposited onto the Si wafer. Fig. 3 shows representative SEM images of the surface morphology of the Si substrates. For oxidation at the relatively low temperatures of 300 °C and 400 °C (i.e., below the melting temperature of Zn, 420 °C), the silicon surfaces are clean without any ZnO nanostructure formation. For oxidation at the temperatures of 500 °C and 800 °C, which are between the melting and boiling points of Zn, discontinuous ZnO thin films are formed on the Si surface and the oxide films become more continuous at the higher temperature (note that the Si surfaces do not show any ZnO nanowire structures except for the observed ZnO thin films). For the oxidation at 1000 °C, there is a high density of ZnO nano-tetrapods formed on the Si surface. As seen in Fig. 3(f), each ZnO nano-tetrapod contains four legs with a diameter of ~500 nm and the length of ~2 μm. The legs have smooth surface and a sharp tip at the end.

It is reasonable to assume that the formation of ZnO thin films on the silicon substrates is due to deposition of ZnO formed from oxidation of Zn vaporized from the Zn foil. The barely visible ZnO formation on the Si substrate for oxidation at 300 °C and 400 °C suggests that very few Zn is vaporized and ZnO forms directly on the Zn foil via the solid–solid transformation (i.e., solid Zn is oxidized to form a solid ZnO coating on the Zn substrate). For oxidation at the temperatures (i.e., 500 °C, 600 °C, and 800 °C examined in our experiments) above the melting point of Zn, a liquid Zn layer should form on the surface of the Zn foil, which promotes the evaporation of Zn. The reaction of Zn vapor and oxygen results in the formation of solid ZnO powders which are

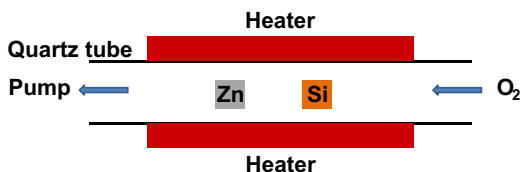


Fig. 1. Schematic illustration of the experimental setup for the oxidation of Zn.

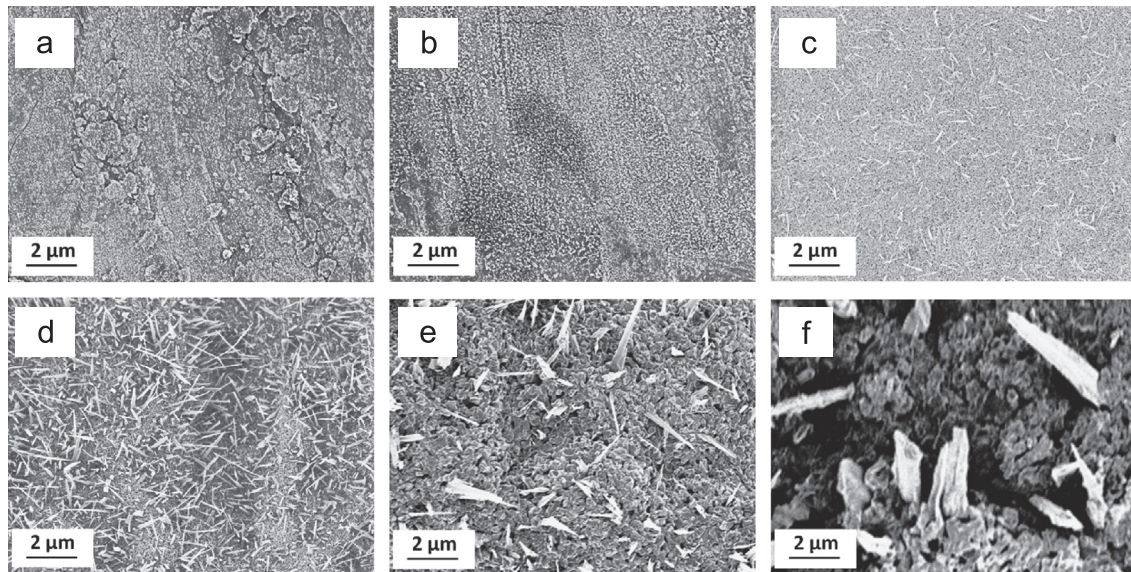


Fig. 2. Representative SEM images of the Zn surfaces oxidized at different temperatures: (a) 200 °C, (b) 300 °C, (c) 400 °C, (d) 500 °C, (e) 600 °C, and (f) 800 °C.

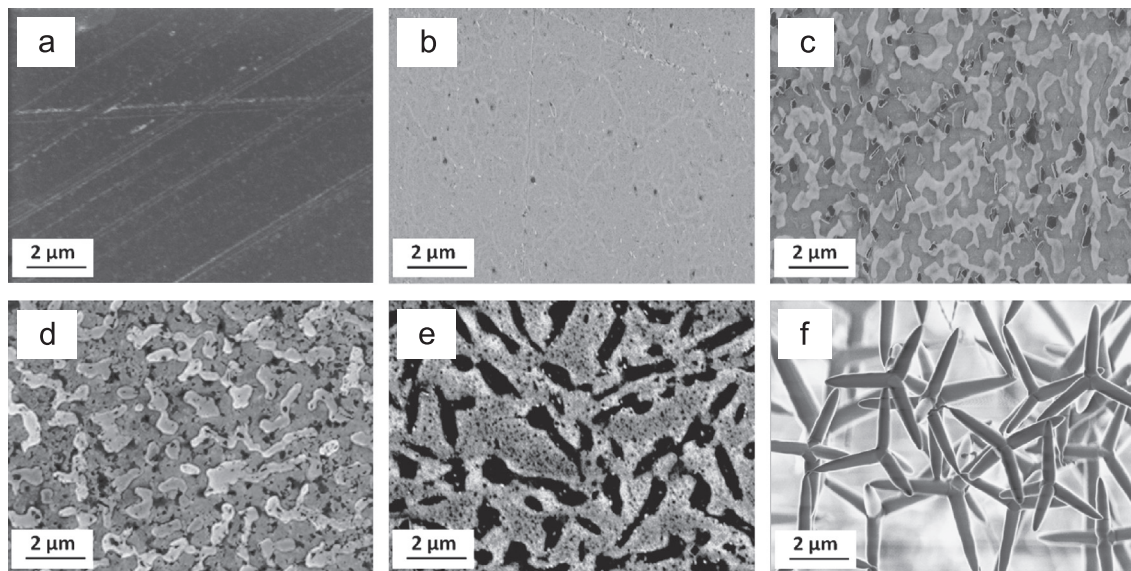


Fig. 3. SEM images of the Si substrates placed next to the Zn foils oxidized at (a) 300 °C, (b) 400 °C, (c) 500 °C, (d) 600 °C, (e) 800 °C, and (f) 1000 °C.

then deposited onto the surrounding area including the Si surface. Increasing oxidation temperature results in more Zn evaporated from the Zn foil and therefore more ZnO deposited on the Si surface. This can also be evidenced by measuring the thickness of the Zn foils oxidized at the different temperatures. As shown in Fig. 4, the thickness of the oxidized Zn foils first increases with increasing the oxidation temperature, and then starts to decrease for oxidation at the temperatures above the melting point. The Pilling–Bedworth ratio (PBR), $PBR = (\text{volume of formed oxide}) / (\text{volume of consumed metal})$, is 1.58 for ZnO formation from the oxidation of Zn, i.e., the volume of the oxide formed is larger than that of the metal consumed. Therefore, for oxidation below the melting point of Zn, the oxide is directly formed on the Zn substrate, which results in the increased total thickness of the oxidized Zn foil. For oxidation above the melting point of Zn, some of the Zn is evaporated from melted Zn to form ZnO powder which is taken away by the gas flow, therefore, the total thickness of the oxidized Zn foil becomes thinner (note that the oxidation at 1000 °C results in complete evaporation of the original Zn foil in the ceramic boat).

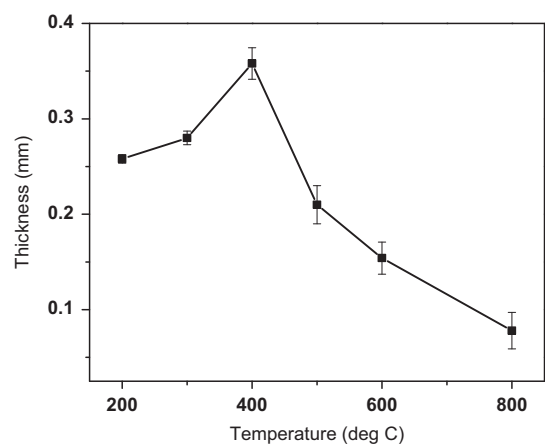


Fig. 4. Dependence of the sample thickness (including the Zn substrate and the ZnO layer formed from the oxidation) on oxidation temperature. Note that the original thickness of the Zn foils before being subjected to oxidation is 0.25 mm.

It becomes evident from the above observations that the ZnO formation occurs via three different mechanisms, depending on the oxidation temperature. For oxidation at the temperatures below the melting point of Zn, the oxide forms via a solid–solid transformation resulting in the growth of a ZnO overlayer on the Zn substrate with formation of ZnO nanowires on the ZnO overlayer. For oxidation at the temperature above the boiling point of Zn, ZnO formation occurs via the vapor–solid transformation in which Zn evaporates from the Zn foil and reacts with oxygen to form ZnO tetrapods which are deposited onto the surrounding area (including the Si wafer). For oxidation at the temperatures between the melting and boiling points of Zn, two mechanisms operate simultaneously for ZnO formation. One is the liquid–solid mechanism that results in the growth of ZnO nanowires directly on the Zn substrate and the other is the vapor–solid mechanism that leads to the formation of ZnO powder that is deposited onto the adjacent Si wafer due to evaporation of Zn from the melted Zn.

To further confirm the temperature effect on the ZnO nanostructure growth described above, detailed transmission electron microscopy (TEM) characterization of the microstructure of the ZnO nanostructures formed at the different temperatures is performed. Fig. 5(a) shows a TEM image of a single ZnO nanowire formed on the Zn foil oxidized at 400 °C. It reveals that the ZnO nanowire contains a bi-crystal boundary at the middle and along the axial direction, as indicated by the white arrows. The high-resolution TEM (HRTEM) image shown in Fig. 5(b) further confirms the bicrystalline structure of the ZnO nanowire. The interplanar spacings of each side of the bicrystalline nanowire as measured from the high-resolution TEM image are both 2.82 Å, corresponding to the calculated lattice spacings of ZnO $\{10\bar{1}0\}$. A large number of ZnO nanowires were examined using HRTEM, and most nanowires formed from the oxidation at the temperatures below the melting point of Zn exhibit the similar bicrystalline structure. Fig. 5(c) shows an SEM image revealing the growth

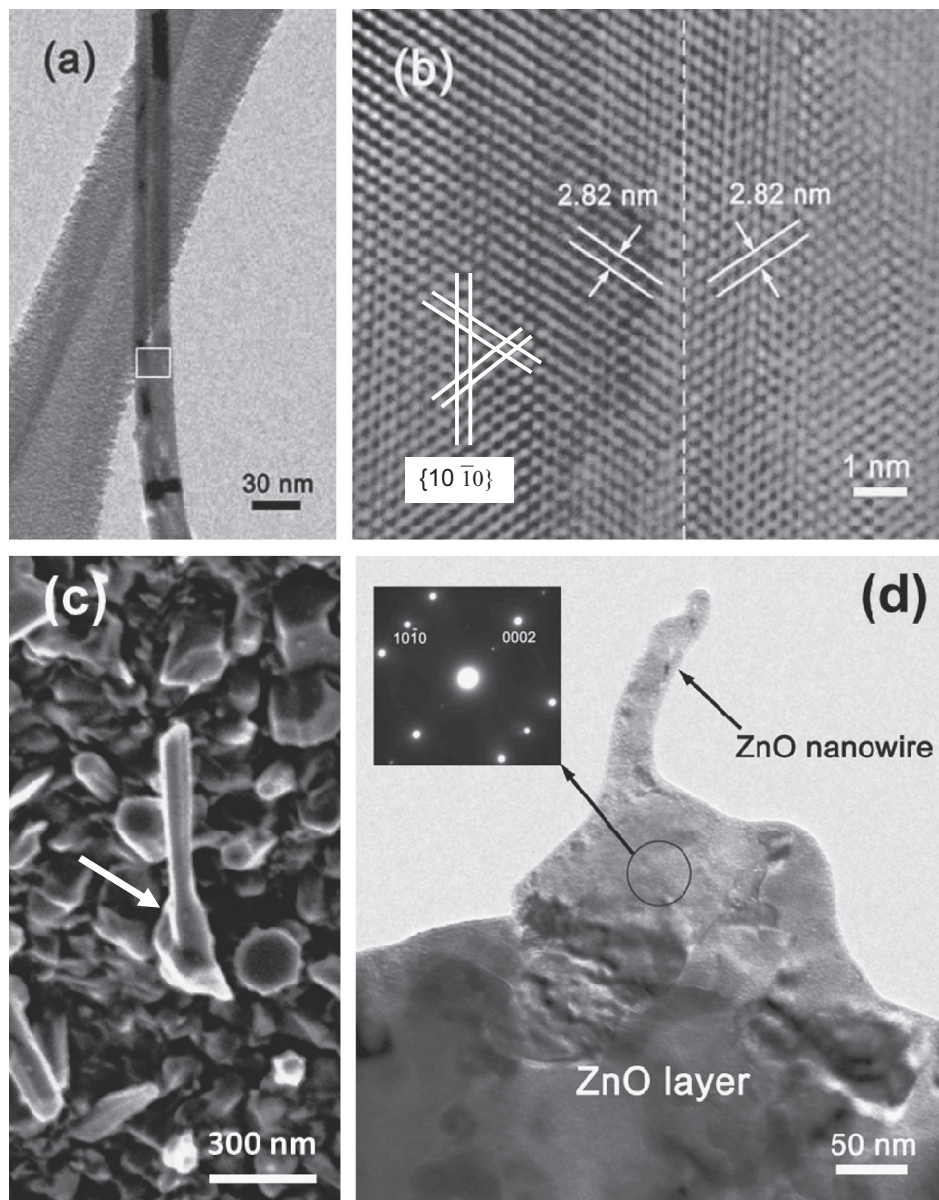


Fig. 5. (a) TEM image of a single ZnO nanowire formed from the oxidation at 400 °C showing the presence of a bicrystalline boundary along the axial direction; (b) HRTEM image obtained from the rectangle area shown in (a); (c) SEM micrograph of a Zn substrate oxidized at 400 °C, showing the initial growth morphology of ZnO nanowires; and (d) Cross-sectional TEM image showing the root region of a ZnO nanowire and the underlying ZnO grain on which the nanowire is grown.

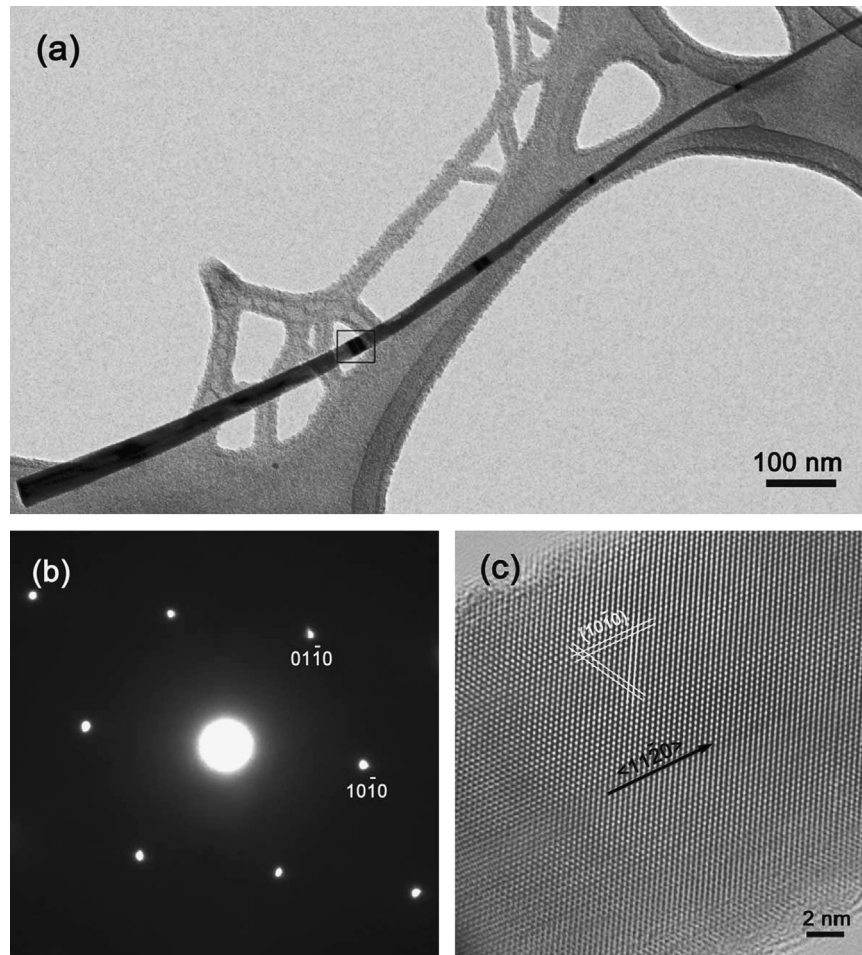


Fig. 6. (a) TEM image of a single ZnO nanowire formed from the oxidation of Zn at 500 °C; (b) SAED pattern of the ZnO nanowire; and (c) HRTEM image obtained from the rectangle area shown in (a).

roots of the nanowires and one can see that the oxidized Zn surface consists of faceted ZnO grains, and ZnO nanowires are grown directly on top of the grains as indicated by the arrow. This growth feature is also confirmed by the cross-sectional TEM image as shown in Fig. 5(d), which demonstrates that the nanowire is formed directly on top of an underlying ZnO grain.

Fig. 6 shows TEM images of a single ZnO nanowire formed on a Zn foil oxidized at 500 °C. Clearly, the nanowire has a needle shape with a diameter of 80 nm at the root and 20 nm at the tip (Fig. 6(a)). Different from the nanowires formed from the oxidation at 400 °C, the TEM image shows that there is no bi-crystal boundary present along the axial direction of the nanowire. This is confirmed by selected area electron diffraction (SAED) pattern as shown in Fig. 6 (b), where the zone axis is along ZnO [0001] direction and the pattern can be identified as single-crystal ZnO. Fig. 6(c) displays an HRTEM image, which reveals that the nanowire is single crystalline without the presence of bi-crystal boundaries along the axial axis. TEM examinations of ZnO nanowires formed from the oxidation at 600 °C and 800 °C reveal the similar structure feature, i.e., no bi-crystal boundary present in the nanowires. These TEM observations are also consistent with other published results [27,32].

Fig. 7(a) shows a TEM image of a ZnO nano-tetrapod formed on the silicon substrate from the oxidation at 1000 °C. Fig. 7(b) is a HRTEM image of a single leg of the ZnO nano-tetrapod shown in Fig. 7(a). The crystal lattice fringes indicate the nano-tetrapod leg has a single crystalline structure and grows along the [0001] direction. The SAED pattern obtained from the nano-tetrapod leg

further confirms its single crystalline structure. By combining the TEM results as shown in Figs. 5–7, we can conclude that oxidation at the temperatures below the melting point of Zn results in the formation of bicrystalline ZnO nanowires, and the oxidation above the melting point leads to formation of single crystalline ZnO nanowires and ZnO tetrapods with single crystalline legs.

4. Discussion

The experimental results described above reveal clearly that the growth morphologies and microstructures of the ZnO nanostructures depend on the oxidation temperature. This can be attributed to the temperature-dependent growth mechanisms, as summarized schematically in Fig. 8. We first discuss the formation of ZnO nanowires for oxidation at the temperatures below the melting point of Zn. For the solid–solid transformation induced oxide nanowire formation during the oxidation of metals, it has been shown that the oxide nanowire formation is driven by relaxation of compressive stresses accumulated in the oxide overlayers and oxide nanowires formed by this mechanism typically show the presence of a bi-crystal boundary along the nanowire axial direction [36–41]. In this mechanism, the compressive stress driving the oxide nanowire formation is originated from the metal–oxide interface for single oxide layer growth or the oxide–oxide interface during layered oxide growth (if the metal has multiple oxide phases, e.g., Cu, Fe) due to their volume mismatch associated with the interfacial conversion reaction.

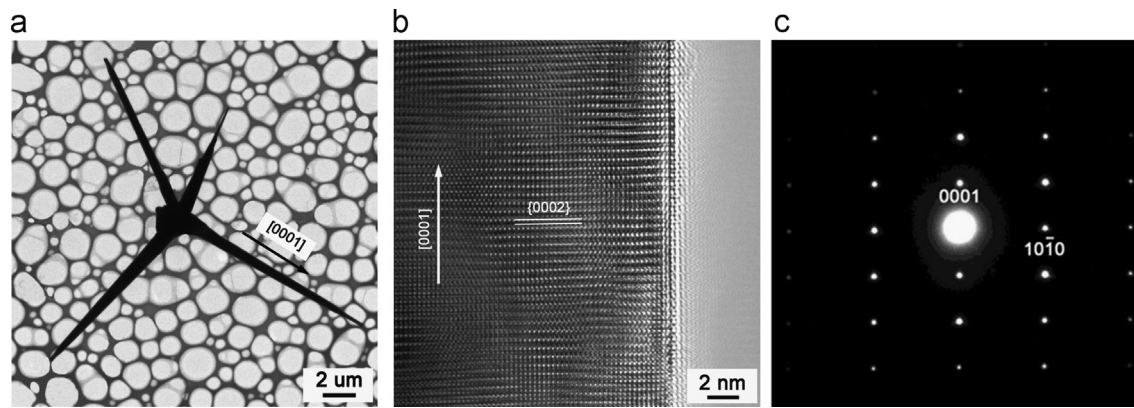


Fig. 7. (a) TEM image of a single ZnO nano-tetrapod formed from the oxidation at 1000 °C; (b) HRTEM image of a single leg of the tetrapod; and (c) SAED pattern obtained from the single leg.

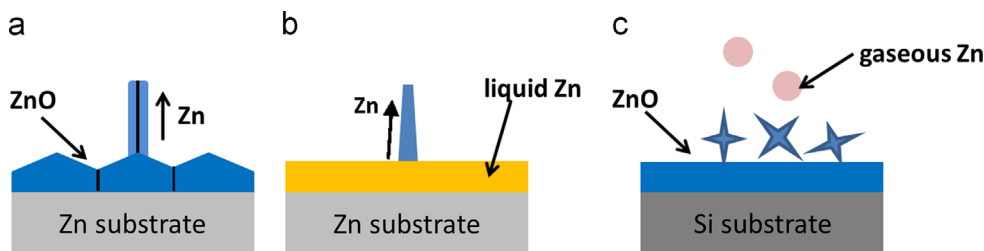


Fig. 8. The different formation processes of ZnO nanostructures at different oxidation temperatures: (a) Solid–solid transformation mechanism for oxidation at temperatures below the melting point of Zn, i.e. $T < 420$ °C; (b) Liquid–solid mechanism for oxidation at temperatures between the melting and boiling points of Zn, i.e. 420 °C $< T < 907$ °C; (c) Vapor–solid mechanism for oxidation at temperatures above the boiling point of Zn, i.e. $T > 907$ °C.

The observed ZnO nanowire formation for the oxidation of Zn at the temperature below its melting point can be understood similarly by the stress-driven mechanism. Owing to the larger molar volume of ZnO than Zn, the transformation of Zn to ZnO generates compressive stress in the ZnO layer adjacent to the ZnO–Zn interface. Since the outer surface of the ZnO layer is stress free, there is a stress gradient across the ZnO layer that drives outward diffusion of Zn ions from the high stress ZnO/Zn interface region to the low stress region of the outer surface for nucleation and growth of ZnO nanowires on exposed ZnO grains. ZnO crystals grown on the adjacent facets of a single ZnO grain are joined to form a bi-crystal structure. As described in Fig. 5, the two sides of bicrystalline nanowires have the same type of $\{10\bar{1}0\}$ lattice. Since ZnO nanowires grow directly on the exposed surfaces of ZnO grains which serve as the structure template for the nucleation and growth of $\{10\bar{1}0\}$ bicrystalline nanowires, the typically observed lattice planes of $\{10\bar{1}0\}$ in the nanowires suggest that the exposed surfaces of the ZnO grains are dominated by $\{10\bar{1}0\}$. This is very likely because the $\{10\bar{1}0\}$ facet has the smallest surface energy among the ZnO surfaces [42]. Further growth of the nanowires occurs via the reaction of Zn ions with oxygen on the nanowire tip, where Zn ions are supplied by surface diffusion along the nanowire wall from the bottom to the tip. Fig. 8 (a) shows schematically the growth process of a bicrystalline ZnO nanowire by this mechanism.

For this mechanism to be operative effectively, the underlying ZnO layer should be sufficiently thin. Our earlier experiments on the oxidation of Cu and Fe showed that the thickness of the top oxide layer (CuO or Fe₂O₃) is less than 1 μm for CuO or Fe₂O₃ nanowire formation [39,41,43]. Otherwise, the stress will be released by other mechanisms such as cracking and delamination of the oxide layer and/or plastic deformation of the oxide and metal substrate if a thick oxide scale develops. This was also confirmed from the oxidation of brass at different temperatures, which showed that the thickening of the underlying ZnO layer

suppresses the formation of ZnO nanowires on the outer surface [37]. For oxidation of Zn at the relatively low temperature (400 °C), the thickness of the underlying ZnO layer on which the formation of ZnO nanowires occurs is only about 150 nm (see Fig. 9(a)). This is consistent with the stress-driven mechanism, which requires that the oxide layer be thin enough for effective relaxation of stresses generated at the ZnO/Zn interface. While for Zn oxidation at temperature above the melting temperature (500–800 °C), we also observed ZnO nanowire formation on the thick ZnO layer, where the thickness of the underlying ZnO layer on the Zn substrate varies from 1.2 μm to 1.8 μm (see Fig. 9(b) and (c)). With such a thick ZnO layer, there is still ZnO nanowire formation and the oxide layers also show good adhesion to the Zn substrate without the oxide delamination or crack formation, as seen from the cross-sectional SEM images shown in Fig. 9(b) and (c). This implies that the ZnO nanowire formation at the temperatures above the melting point follows a different mechanism.

For oxidation at temperatures between the melting and boiling points of Zn, the oxide nanowire formation on the Zn substrate can be attributed to a liquid–solid process. At these temperatures, the Zn substrate surface forms a thin layer of liquid Zn. Reaction of the liquid Zn with incoming oxygen forms solid ZnO nuclei on the liquid Zn layer (note that ZnO has a melting point of around 1970 °C and forms as solid precipitates during the oxidation), which serve as seeds for ZnO nanowire formation [27]. The tapered shape of the nanowires (see Fig. 6(a)) suggests that the nanowire growth occurs via surface diffusion of Zn ions along the side wall of the nanowire, which results in simultaneous growth in both the axial and radial directions by reacting with impinging oxygen. The surface diffusion of Zn is driven by the concentration gradients of Zn ions along the nanowire wall from the root region to the tip. This also explains why most nanowires have a coarse root and become thinner at the tip because a significant amount of Zn ions are incorporated into the nanowire near the root region by reacting with impinging oxygen.

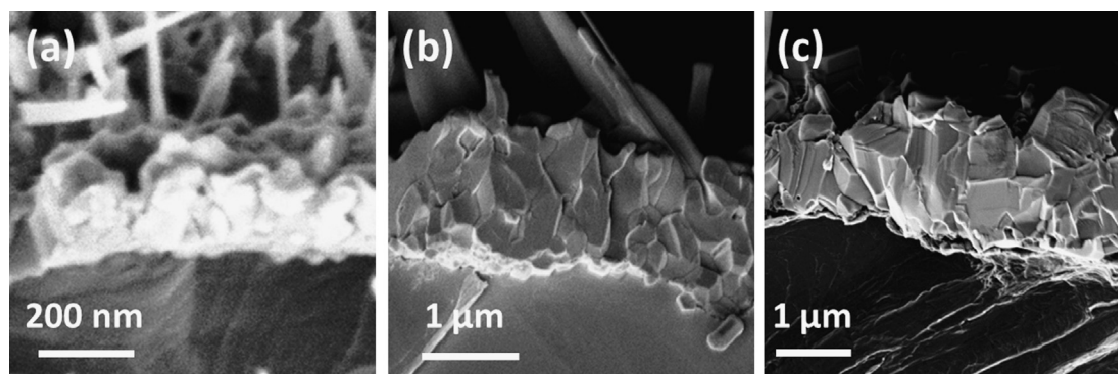


Fig. 9. Cross-sectional SEM images revealing the thicknesses of the underlying ZnO layers formed on the Zn substrates oxidized at different temperatures: (a) 400 °C; (b) 600 °C; and (c) 800 °C.

At temperature above the boiling temperature of Zn, the formation of ZnO nano-tetrapods is observed as shown in Fig. 7. The growth of ZnO tetrapods have also been observed previously from the oxidation at the similar high temperature [14,44]. The vapor–solid mechanism can be employed to understand the formation of the tetrapod morphology. The Zn substrate rapidly evaporates to form Zn vapor above the boiling temperature. With the inlet flow of oxygen gas, ZnO nuclei start to form by the reaction between Zn vapor and oxygen. It was suggested that ZnO nuclei formed from the vapor reaction adopt an octahedral-twinned shape with exposed (0001) base planes, which minimize the surface energy of the ZnO cluster because of the low surface energy of the basal plane (the surface energy for Zn-terminated base (0001) surface is slightly larger than the (10 $\bar{1}$ 0) plane) [42,45]. However, after the octahedral multiple twins grow to a larger size, the strain energy due to the misfit angle of the multiple twins leads to the cracking of the twin boundaries and the subsequent growth of the ZnO particle continues preferentially along the [0001] direction due to the larger anisotropy of the growth rate. As a result, a tetrapod ZnO nanostructure is formed by filling up the crack in the octahedral-twinned nucleus, and the variation in the cracking process in octahedral-twinned nucleus may lead to variation in the angles among legs of the ZnO tetrapods. Such a process of tetrapod ZnO formation has been described previously in the literature [44–47]. This mechanism corroborates with our TEM observations of the ZnO tetrapods, which reveal that the axial direction of tetrapod legs is indeed along ZnO [0001] direction, as shown in Fig. 7.

5. Conclusions

The growth morphologies and microstructure of ZnO nanostructures formed from the oxidation of Zn at different temperatures are studied. It is shown that the oxidation below the melting point of Zn results in the growth of bicrystalline ZnO nanowires, single-crystalline ZnO nanowires between the melting and boiling points of Zn, and ZnO tetrapods above the boiling point of Zn. The temperature-dependent growth morphology and microstructure are attributed to the temperature effect on the oxidation mechanism of Zn. For oxidation below the melting point of Zn, the ZnO nanowire formation follows a solid–solid transformation mechanism in which the compressive stress generated from the ZnO/Zn interfacial reaction stimulates ZnO nanowire formation. At temperatures between the melting and boiling temperatures of Zn, the formation of single crystalline nanowire occurs via a liquid–solid mechanism in which liquid Zn reacts with gaseous oxygen to form solid ZnO nuclei that grow anisotropically via surface diffusion of Zn. The formation of ZnO nano-tetrapods at the temperature

above the boiling temperature of Zn follow a vapor–solid mechanism in which the tetrapod ZnO growth occurs by filling up cracks in octahedral-twinned nuclei.

Acknowledgments

This work was supported by the National Science Foundation under Grant no. CMMI-0825737. Y.Q. Wang would like to thank the financial support from the Natural Science Foundation for Outstanding Young Scientists in Shandong Province, China (Grant no JQ201002). We thank Mr. Shawn Wagoner for the help with gold deposition on Si.

References

- [1] Z.L. Wang, ZnO nanowire and nanobelt platform for nanotechnology, *Mater. Sci. Eng.: R: Rep.* 64 (3–4) (2009) 33–71.
- [2] U. Ozgur, Y.I. Alivov, C. Liu, A. Teke, M. Reshchikov, S. Dogan, V. Avrutin, S.-J. Cho, H. Morkoc, A comprehensive review of ZnO materials and devices, *J. Appl. Phys.* 98 (4) (2005) 041301–041303.
- [3] G.-C. Yi, C. Wang, W.I. Park, ZnO nanorods: synthesis, characterization and applications, *Semicond. Sci. Technol.* 20 (4) (2005) S22.
- [4] T. Zhai, X. Fang, M. Liao, X. Xu, H. Zeng, B. Yoshio, D. Golberg, A comprehensive review of one-dimensional metal oxide nanostructure photodetectors, *Sensors* 9 (8) (2009) 6504–6529.
- [5] C.L. Tang, C.M. Jiang, W.Q. Lu, J.H. Song, Nonlinear length dependent electrical resistance of a single crystal zinc oxide micro/nanobelt, *Phys. Chem. Chem. Phys.* 15 (21) (2013) 8222–8227.
- [6] H. Wan, H.E. Ruda, A study of the growth mechanism of CVD-grown ZnO nanowires, *J. Mater. Sci.: Mater. Electron.* 21 (10) (2010) 1014–1019.
- [7] P.X. Gao, Z.L. Wang, Self-assembled nanowire-nanoribbon junction arrays of ZnO, *J. Phys. Chem. B* 106 (49) (2002) 12653–12658.
- [8] X.D. Wang, J.H. Song, Z.L. Wang, Nanowire and nanobelt arrays of zinc oxide from synthesis to properties and to novel devices, *J. Mater. Chem.* 17 (8) (2007) 711.
- [9] D. Chu, Y. Masuda, T. Ohji, K. Kato, Formation and photocatalytic application of ZnO nanotubes using aqueous solution, *Langmuir* 26 (4) (2009) 2811–2815.
- [10] H. Yu, Z. Zhang, M. Han, X. Hao, F. Zhu, A general low-temperature route for large-scale fabrication of highly oriented ZnO nanorod/nanotube arrays, *J. Am. Chem. Soc.* 127 (8) (2005) 2378–2379.
- [11] P.X. Gao, Z.L. Wang, High yield synthesis of single crystal nanosprings of ZnO, *Small* 1 (10) (2005) 945–949.
- [12] Y. Ding, X.Y. Kong, Z.L. Wang, Doping and planar defects in the formation of single-crystal ZnO nanorings, *Phys. Rev. B* 70 (23) (2004) 235408.
- [13] S.S. Tneh, H. Abu Hassan, K.G. Saw, F.K. Yam, Z. Hassan, Structural and optical properties of large-scale ZnO nanowires and nanosheets prepared by dry thermal oxidation, *Surf. Rev. Lett.* 16 (6) (2009) 901–904.
- [14] W.D. Yu, X.M. Li, X.D. Gao, Self-catalytic synthesis and photoluminescence of ZnO nanostructures on ZnO nanocrystal substrates, *Appl. Phys. Lett.* 84 (14) (2004) 2658.
- [15] Y. Dai, Y. Zhang, Z.L. Wang, The octa-twin tetraleg ZnO nanostructures, *Solid State Commun.* 126 (11) (2003) 629–633.
- [16] J. Li, H. Peng, J. Liu, H.O. Everitt, Facile gram-scale growth of single-crystalline nanotetrapod-assembled ZnO through a rapid process, *Eur. J. Inorg. Chem.* 2008 (20) (2008) 3172–3176.
- [17] J. Li, Q. Zhang, H. Peng, H.O. Everitt, L. Qin, J. Liu, Diameter controlled vapor–solid epitaxial growth and properties of aligned ZnO nanowire arrays, *J. Phys. Chem. C* 113 (10) (2009) 3950–3954.

- [18] W. Lu, C. Jiang, D. Caudle, C. Tang, Q. Sun, J. Xu, J. Song, Lateral growth of zinc oxide nanorod arrays on silicon electrodes by catalyst-free vapor solid process—a technique for growing nanocircuits, *Phys. Chem. Chem. Phys.* 15 (2013) 13532–13537.
- [19] W.I. Park, D.H. Kim, S.-W. Jung, G.-C. Yi, Metalorganic vapor-phase epitaxial growth of vertically well-aligned ZnO nanorods, *Appl. Phys. Lett.* 80 (2002) 4232.
- [20] S. Sahoo, J. Scott, A. Arora, R.S. Katiyar, Self assembled highly uniform ZnO submicrometer rods on metal grid grown by vapor–liquid–solid method, *Cryst. Growth Des.* 11 (8) (2011) 3642–3647.
- [21] Y.R. Lin, Y.K. Tseng, S.S. Yang, S.T. Wu, C.L. Hsu, S.J. Chang, Buffer-facilitated epitaxial growth of ZnO nanowire, *Cryst. Growth Des.* 5 (2) (2005) 579–583.
- [22] J. Song, S.A. Kulinich, J. Yan, Z. Li, J. He, C. Kan, H. Zeng, Epitaxial ZnO nanowire-on-nanoplate structures as efficient and transferable field emitters, *Adv. Mater.* 25 (40) (2013) 5750–5755.
- [23] W.C. Jin, S.L. Churl, I.L. Kyoung, M.K. Seon, H.K. Sung, K.K. Young, Morphology and electrical properties of high aspect ratio ZnO nanowires grown by hydrothermal method without repeated batch process, *Appl. Phys. Lett.* 101 (8) (2012) 083905–083905-4.
- [24] L. Vayssieres, Growth of arrayed nanorods and nanowires of ZnO from aqueous solutions, *Adv. Mater.* 15 (5) (2003) 464–466.
- [25] S. Ren, Y.F. Bai, J. Chen, S.Z. Deng, N.S. Xu, Q.B. Wu, S. Yang, Catalyst-free synthesis of ZnO nanowire arrays on zinc substrate by low temperature thermal oxidation, *Mater. Lett.* 61 (3) (2007) 666–670.
- [26] X. Wen, Y. Fang, Q. Pang, C. Yang, J. Wang, W. Ge, K.S. Wong, S. Yang, ZnO nanobelt arrays grown directly from and on zinc substrates: synthesis, characterization, and applications, *J. Phys. Chem. B* 109 (2005) 15303–15308.
- [27] H. Dang, J.S.F. Wang, The synthesis of metal oxide nanowires by directly heating metal samples in appropriate oxygen atmospheres, *Nanotechnology* 14 (2003) 738–741.
- [28] Y.H. Sun, J.Y. Gao, R. Zhu, J. Xu, L. Chen, J.M. Zhang, Q. Zhao, D.P. Yu, In situ observation of ZnO nanowire growth on zinc film in environmental scanning electron microscope, *J. Chem. Phys.* 132 (12) (2010) 124705.
- [29] H.Z. Zhang, X.C. Sun, R.M. Wang, D.P. Yu, Growth and formation mechanism of c-oriented ZnO nanorod arrays deposited on glass, *J. Cryst. Growth* 269 (2–4) (2004) 464–471.
- [30] Q. Zhao, J.Y. Gao, R. Zhu, T.C. Cai, S. Wang, X.F. Song, Z.M. Liao, X.H. Chen, D.P. Yu, Ultrahigh field emission current density from nitrogen-implanted ZnO nanowires, *Nanotechnology* 21 (9) (2010) 095701.
- [31] Y.H. Sun, Q. Zhao, J.Y. Gao, R. Zhu, X.W. Wang, J. Xu, L. Chen, J.M. Zhang, D.P. Yu, Growth mechanism study via in situ epitaxial growth of high-oriented ZnO nanowires, *CrystEngComm* 13 (2) (2011) 606.
- [32] H. Liang, L. Pan, Z. Liu, Synthesis and photoluminescence properties of ZnO nanowires and nanorods by thermal oxidation of Zn precursors, *Mater. Lett.* 62 (12–13) (2008) 1797–1800.
- [33] F. Fang, D.X. Zhao, J.Y. Zhang, D.Z. Shen, Y.M. Lu, X.W. Fan, B.H. Li, X.H. Wang, The influence of growth temperature on ZnO nanowires, *Mater. Lett.* 62 (6–7) (2008) 1092–1095.
- [34] R. Palumbo, J. Lede, O. Boutin, E. Elorza Ricart, A. Steinfeld, S. Möller, A. Weidenkaff, E. Fletcher, J. Bielikki, The production of Zn from ZnO in a high-temperature solar decomposition quench process—I. The scientific framework for the process, *Chem. Eng. Sci.* 53 (14) (1998) 2503–2517.
- [35] C.X. Zhao, Y.F. Li, J. Zhou, L.Y. Li, S.Z. Deng, N.S. Xu, J. Chen, Large-scale synthesis of bicrystalline ZnO nanowire arrays by thermal oxidation of zinc film: growth mechanism and high-performance field emission, *Cryst. Growth Des.* 13 (7) (2013) 2897–2905.
- [36] F. Morin, Copious whisker growth on copper scale, *J. Mater. Sci. Lett.* 2 (7) (1983) 383–384.
- [37] L. Yuan, C. Wang, R.S. Cai, Y.Q. Wang, G.W. Zhou, Spontaneous ZnO nanowire formation during oxidation of Cu–Zn alloy, *J. Appl. Phys.* 114 (2) (2013) 023512–023518.
- [38] L. Yuan, G.W. Zhou, Enhanced CuO nanowire formation by thermal oxidation of roughened copper, *J. Electrochem. Soc.* 159 (4) (2012) C1.
- [39] L. Yuan, Y.Q. Wang, R.S. Cai, Q.K. Jiang, J.B. Wang, B.Q. Li, A. Sharma, G.W. Zhou, The origin of hematite nanowire growth during the thermal oxidation of iron, *Mater. Sci. Eng.: B* 177 (2012) 327–336.
- [40] R. Mema, L. Yuan, Q.T. Du, Y.Q. Wang, G.W. Zhou, Effect of surface stresses on CuO nanowire growth in the thermal oxidation of copper, *Chem. Phys. Lett.* 512 (1–3) (2011) 87–91.
- [41] L. Yuan, Y.Q. Wang, R. Mema, G.W. Zhou, Driving force and growth mechanism for spontaneous oxide nanowire formation during the thermal oxidation of metals, *Acta Mater.* 59 (6) (2011) 2491–2500.
- [42] U. Diebold, L.V. Koplitz, O. Dulub, Atomic-scale properties of low-index ZnO surfaces, *Appl. Surf. Sci.* 237 (1) (2004) 336–342.
- [43] L. Yuan, Q.K. Jiang, J.B. Wang, G.W. Zhou, The growth of hematite nanobelts and nanowires—tune the shape via oxygen gas pressure, *J. Mater. Res.* 27 (7) (2012) 1014–1021.
- [44] L. Feng, A. Liu, M. Liu, Y. Ma, J. Wei, B. Man, Fabrication and characterization of tetrapod-like ZnO nanostructures prepared by catalyst-free thermal evaporation, *Mater. Charact.* 61 (1) (2010) 128–133.
- [45] H. Iwanaga, M. Fujii, S. Takeuchi, Growth model of tetrapod zinc oxide particles, *J. Cryst. Growth* 134 (3) (1993) 275–280.
- [46] S. Takeuchi, H. Iwanaga, M. Fujii, Octahedral multiple-twin model of tetrapod ZnO crystals, *Philos. Mag. A* 69 (6) (1994) 1125–1129.
- [47] M. Shiojiri, C. Kaito, Structure and growth of ZnO smoke particles prepared by gas evaporation technique, *J. Cryst. Growth* 52 (1981) 173–177.